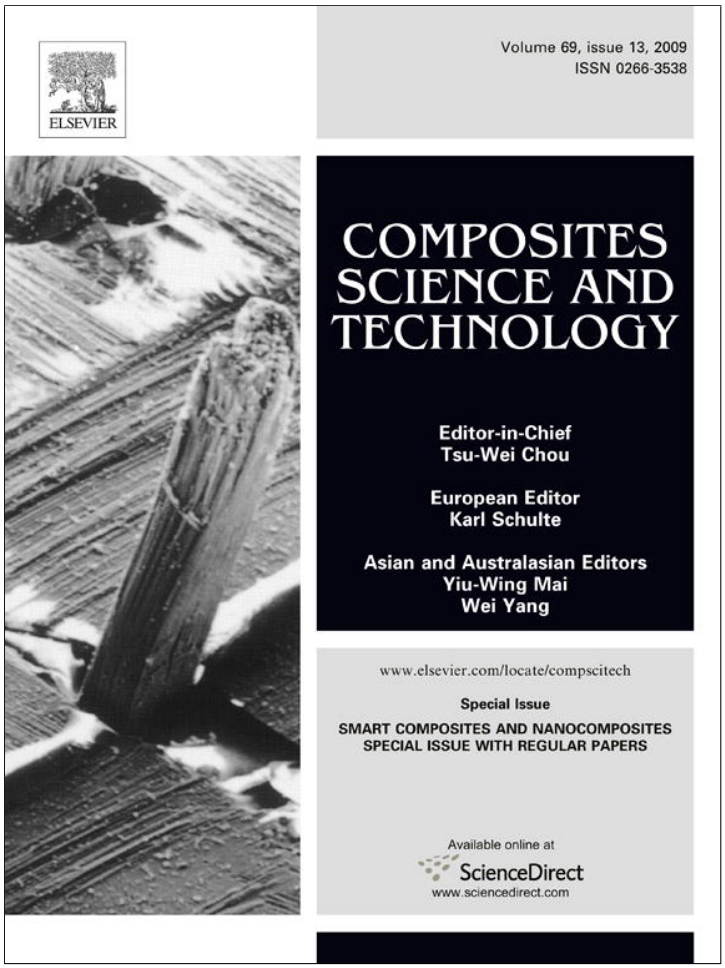

Composites Science and Technology 69 (2009) 2231–2240

Contents lists available at ScienceDirect

Composites Science and Technology

journal homepage: www.elsevier.com/locate/compscitech

Compression strength of sandwich panels with sub-interface damage in the foam core

Vitaly Koissin [a,*], Andrey Shipsha [b,1], Vitaly Skvortsov [a,2]

[a] Dept. of Strength of Materials, State Marine Technical University, 198 262 St.-Petersburg, Russia
[b] Dept. of Aeronautical and Vehicle Engineering, Royal Institute of Technology, S–100 44 Stockholm, Sweden

ARTICLE INFO

Article history:
Received 6 April 2009
Received in revised form 11 June 2009
Accepted 12 June 2009
Available online 21 June 2009

Keywords:
A. Sandwich
B. Local damage
A. Crushed foam
B. Residual dent
C. Local buckling
C. Damage tolerance

ABSTRACT

This paper addresses the effect of a local quasi-static indentation or a low-velocity impact on the residual strength of foam core sandwich panels subjected to edgewise compression. The damage is characterized by a local zone of crushed core accompanied by a residual dent in the face sheet. Experimental studies show that such damage can significantly alter the compressive strength. Theoretical analysis of the face sheet local bending is performed for two typical damage modes (with or without a face–core debonding). The solutions allow estimation of the onset of (a) an unstable dent growth (local buckling) or (b) a compressive failure in the face sheet. The theoretical results are in agreement with the test data for two considered sandwich configurations.

1. Introduction

With the appearance of sandwich structures, the problem of their local bucking become entrenched in the design process, due to a limited support provided by the core layer for the in-plane compressed face sheets. The local buckling (wrinkling) of intact sandwiches has been investigated in many studies, and a number of solutions were proposed, e.g. Rammerstorfer and Vonach [1] and Fagerberg [2]. The less trivial problem is the case of a local damage in the face (delamination, fibre breaks, etc.) or in the core (e.g. a face–core debond), when the residual compressive strength can be much lower than that of an undamaged panel, Hayman [3]. This has also been investigated by many in the past. A detailed review of earlier (until 1997) studies is presented by Olsson in [4], along with a discussion of different failure modes. A number of new studies appeared later, e.g. [5–19], but mainly dealing with experimental and finite-element (FE) results; only [11,15] present analytical failure models.

The present paper extends the previous work by the authors [20–22] on the local buckling in sandwich panels containing a sub-interface damage in the foam core, which locally reduces support for faces. The focus is laid on the core crush damage accompanied by a permanent residual dent in the face sheet, while the laminate itself is considered undamaged. The approach yields simple theoretical solutions for the ultimate (local buckling or compressive failure) stress in the face sheet, even when accounting for the supporting effect of the crushed foam material. The theoretical results are compared with the test data for sandwich panels indented or impacted with a rigid hemisphere. The solutions give satisfactory predictions for the residual compressive strength, with an accuracy acceptable for engineering purposes.

2. Experimental

An experimental study is initially conducted to characterize the local damage and failure features and thus to provide an essential input for the theoretical modelling. Flat specimens (180 × 270 mm in-plane dimensions) with thick rigid foam cores and relatively thin faces are used. The specimens are (1) locally loaded causing a local core crushing and residual dent in the face sheet and then (2) subjected to an edgewise compression, as described below.

2.1. Sandwich configurations

Two sandwich configurations are fabricated using the vacuum-assisted resin transfer moulding. The core materials are Rohacell WF51 or Divinycell H130 rigid closed-cell foams; they can be

* Corresponding author. Present address: Univ. of Twente, Faculty of Engng. Tech., Production Tech., NL–7500AE Enschede, The Netherlands. Tel.: +31 53 489 24 97; fax: +31 53 489 47 84.
E-mail address: vitaly@kth.se (V. Koissin).
[1] Present address: Inspecta Technology AB, S–104 25 Stockholm, Sweden.
[2] This publication is dedicated to the memory of Prof. Vitaly Skvortsov (27.01.1958–26.09.2008) who greatly helped to give birth to the scientific way of the authors.

0266-3538/$ - see front matter © 2009 Elsevier Ltd. All rights reserved.
doi:10.1016/j.compscitech.2009.06.014

treated as isotropic. The face sheets are quasi-isotropic laminates comprised of Devold DBLT850-E10-I (areal weight 835 g/m2) quadriaxial E-glass non-crimp fabric and vinylester resin Norpol Dion 9500. The total lay-up is $[0,-45,90,+45,-45,90,+45,0]_s$ or $[0,45,90,-45]_s$ for configurations # 1 and # 2, respectively. The basic material data are listed in Table 1. The Poisson's ratios are either estimated by laminate theory or taken from the core manufacturers' data sheets [23,24].

2.2. Indentation and impact tests

Indentation tests are conducted at a cross-head rate of 2 mm/min. To limit the overall bending, the sandwich panel is rested on a rigid plate. The load is applied at the specimen centre using a steel hemisphere as shown in Figs. 1a and 2a. A 25 mm hemisphere is used for configuration # 1, and a 50 mm one is used for configuration # 2, since the smaller indentor provokes a premature perforation of the laminate in the latter case. The specimens are indented per 2.4, 3.6, 4.8, and 5.8 mm (configuration # 1) or 1.75, 2, 2.5, 3, 4, 5, and 6 mm (configuration # 2). This maximal indentation magnitude is further denoted as w_0; four specimens are tested for each w_0.

A typical load–displacement curve is shown in Fig. 3 (left). Path *A*–*B* corresponds to a pure elastic response. Core crushing (cell compaction) starts at point *B*, and the following path *B*–*C* exhibits a progressive growth of the core crush zone. Upon unloading, path *C*–*D*, a prominent residual dent is observed in the face sheet, point *D*, mainly as the result of a pull-in action of the crushed core. The maximum magnitude of this dent is measured during 10 min taking the displacement from the testing machine that corresponds to zero load (path *D*–*E*). The dent magnitude decreases by up to 30% during the first minute after the unloading, gradually leveling off; this stable value (at point *E*) is further denoted as w_0^r. The transient instability should be attributed to specific properties of the crushed foam, see Section 2.5.

Instead of the static indentation, a number of configuration # 1 specimens are impacted, using a drop-weight rig and the same loading tip and support conditions. The hemispherical tip is attached to a weighted body providing a total mass of 7.8 kg; the impact energy (10, 20, 30, 40, 50, and 60 J) is defined by the drop

Table 1
Basic mechanical properties of the sandwich constituents.

Configuration	Material	Thickness (mm)	Fibre content (%)	Young's modulus (MPa)	Poisson's ratio	Yield strain	Yield stress (MPa)
# 1	WF51	50	–	85[a]	0.42	0.012[a]	0.9[a]
	GFRP	2.4	55	19,300[b]	0.25	0.002[c]	44.3[c]
# 2	H130	40	–	135[a]	0.32	0.014[a]	2.3[a]
	GFRP	1.6	41	15,800[b]	0.25	0.002[c]	42.8[c]

[a] Out-plane compression (ASTM D1623-78).
[b] In-plane tension (ASTM D638M).
[c] Conventional value, in-plane compression (ASTM D3410).

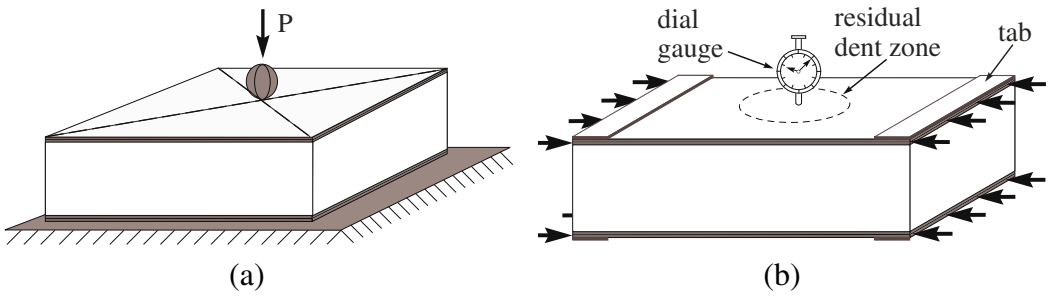

Fig. 1. Schematic of a local indentation (a) and edgewise compression (b) tests.

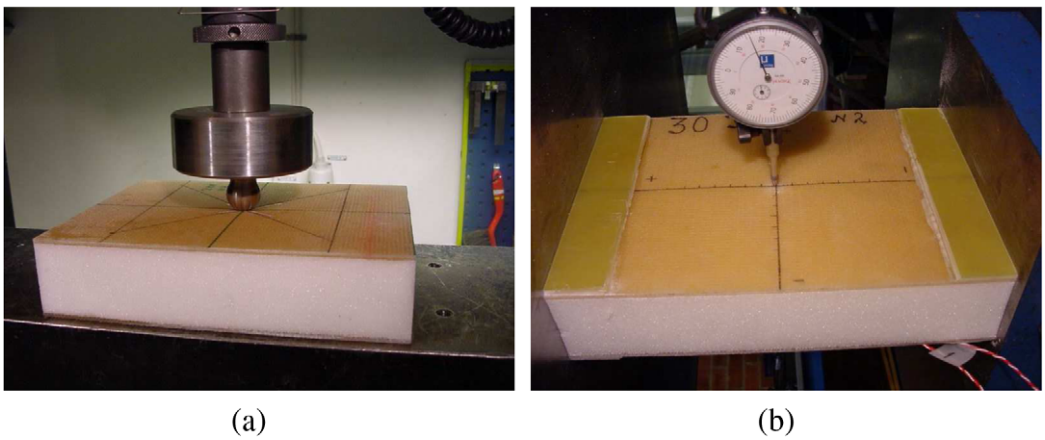

Fig. 2. Configuration # 1 plate subjected to a local indentation (a) or edgewise compression (b).

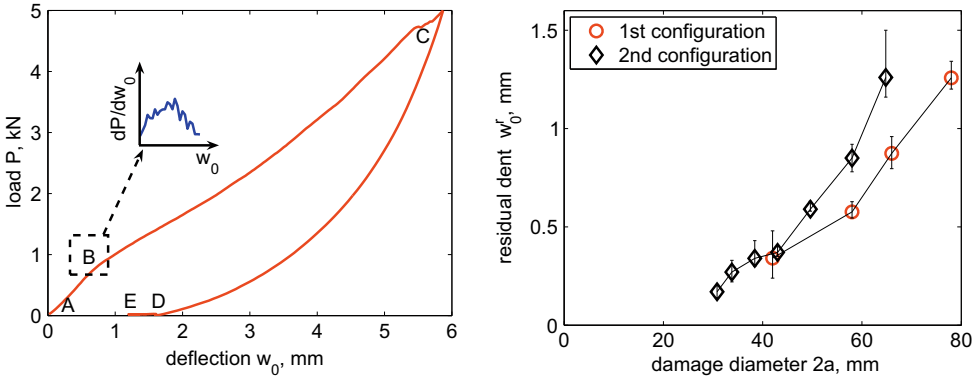

Fig. 3. Applied load vs. face deflection response for configuration # 1 (left) and max. residual dent vs. mean damage diameter for indented specimens (right).

height, assuming the ideal free fall. After rebound, the impactor is captured to avoid a secondary damage of the specimens. Series of 4–5 specimens are tested for each impact energy. Details can be obtained in [20,25].

2.3. Damage characterization

Besides the residual dent, a visual inspection usually reveals a delamination zone (seen as a whitened spot) in the face sheet confined to the contact area with the loading tip. For example, this zone is about 18 mm in diameter after a 60 J impact. No delamination is observed after a 2.5 mm indentation or a 10 J impact. Configuration # 1 panels also contain a plastically deformed zone having smoother surface and slightly different color. Configuration # 2 panels have no such "Brinell-type" damage at the loading site, obviously due to the twice larger indentor tip and more flexible face sheet.

A damage diameter is plotted against the residual dent magnitude in Fig. 3 (right). For configuration # 1 the dent is also quantified by moving a dial gauge along a line crossing the centre, with a 45° step; almost circular in-plane shape is detected. The averaged results are presented in Fig. 4. A distinct drop of the dent profile is attributed to the "Brinell-type" crater mentioned above. It is also noted that the residual dent provides a conservative indication of the sub-interface damage, since the residual dent diameter is somewhat larger than the core crush diameter [4,20].

The core crush zone is hidden under the face sheet, Fig. 5. For configuration # 1, when the face is manually detached in several specimens after indentation, thin crushed foam traces, remained on its inner surface, are good indicator of the damage boundary

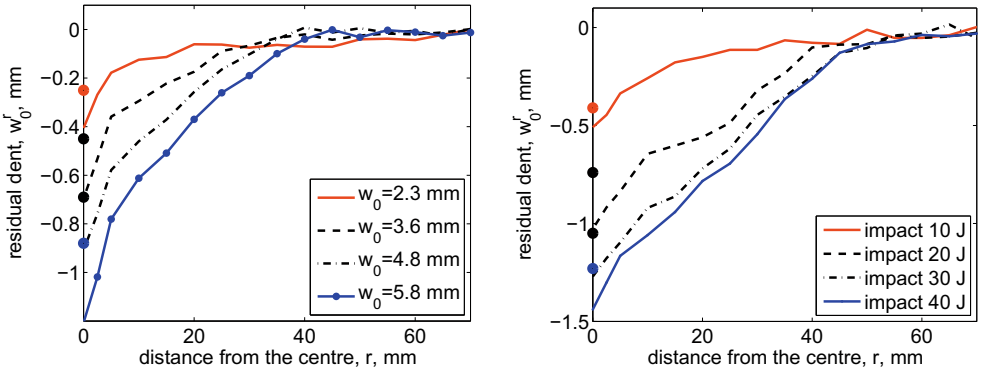

Fig. 4. Profile of the face sheet residual dent in indented (left) or impacted (right) panels of configuration # 1. Measured several days after the tests. Filled dots at $(r = 0)$ denote the estimated maximum residual dent w_0^r without the "Brinell's" component.

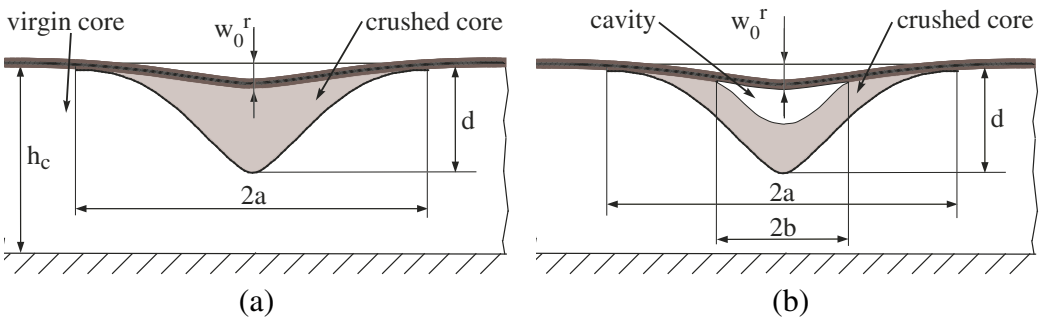

Fig. 5. Schematic of a local damage without (a) or with (b) partial face–crushed core debond.

[20]. This was not the case for configuration # 2; then the core crush boundary was estimated using an FE model reported in [20]. It should be pointed out that a similar damage in configuration # 2 sandwich beams (indented more than for 4 mm) is accompanied by the second crush zone close to the core midplane [25]. In the present study, a 5 mm thick slice is cut across the damage centre of a 6 mm indented panel and projected with X-rays. No second crush zone is detected; its absence can be explained by a milder strain field during the indentation, if compared with the beam specimens.

The impact-induced damage in configuration # 1 specimens differs from the "static" one and consists of two regions, Fig. 5b. In the central part, the face sheet and the crushed core are debonded, while they keep contact in the peripheral region. This cavity appears probably due to a rapid deformation of the foam material during the impact and rebound. The cavity is located some small distance below the face, since the foam cells are strengthened with the resin at the face–core interface. The in-plane cavity diameter, $2b$, is approximately 1/2 of the core crush zone diameter, $2a$. More detailed geometrical characterization of the impact damage is presented in [20,25].

2.4. Edgewise compression

The edgewise compression is performed according to ASTM C364–94, as shown in Figs. 1b and 2b. The shorter edges of the specimens are reinforced with tabs and milled to ensure uniform load transfer and to avoid local yielding of the faces. The specimens are compressed between two steel plates at a displacement rate of 1 mm/min. The compression direction corresponds to the fibre direction in the outermost layers of the face laminate. A dial gauge is used to measure the out-of-plane displacement at the damage centre. One specimen from each series of configuration # 1 is also instrumented with uniaxial strain gauges; details are reported in [20].

Since the laminate stiffness is much larger than that of the core layer, the compressive stress in the faces is calculated using the simplest formula

$$\sigma = P/2h_f b, \tag{1}$$

where P is the load sampled from the press, h_f is the face thickness, and b is the panel width.

The following failure modes are observed, see also Figs. 6 and 7:

Abrupt bifurcation of the face sheet (wrinkling) leading to a complete disintegration of the specimen. This is common for configuration # 1 specimens having a relatively small damage (e.g. the 10 J panels). The wrinkling wave is manifested by the foam core fragments remained on the detached faces.

Failure in the core initiated by the local buckling in the residual dent zone. Configuration # 1 specimens (having a large damage) exhibit a progressive dent growth. Typical dial gauge history sampled for such a specimen is shown in Fig. 8 (left). At a certain moment, the dent growth rate increases that is attributed to the local buckling onset. The final abrupt failure can be caused by the tensile fracture in the core on either side of the dent zone, since a visual observation of the separated face sheet reveals traces of the foam material just at the outer boundary of the core crush zone, Fig. 7b. In this photo the traces are situated across width of panel but often they occur at the damage zone sides oriented along panel.

Typical load curve for this case is shown in Fig. 8 (right). The response is almost linear up to the failure; i.e. the dent growth and non-linear deformation in the face cause a marginal decrease in the panel stiffness. This disagrees with observations for sandwich beams of the same configurations [22]. This is

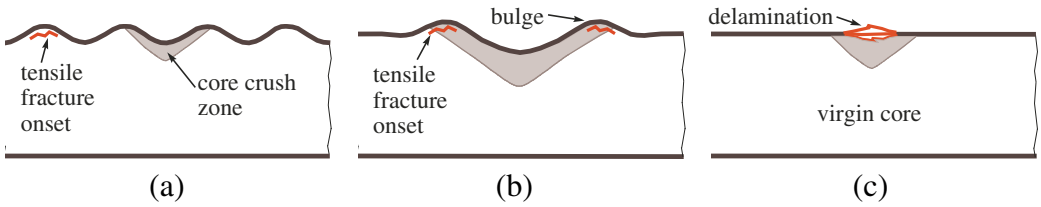

Fig. 6. Failure modes: (a) wrinkling (b) local buckling (c) delamination + kink band formation.

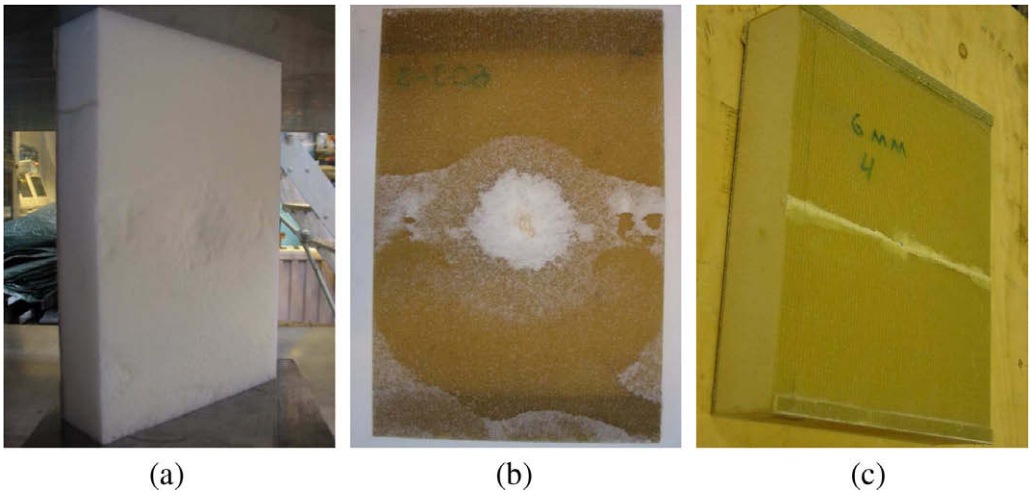

Fig. 7. Typical failure observed for configuration # 1 (a and b) or # 2 (c) panels.

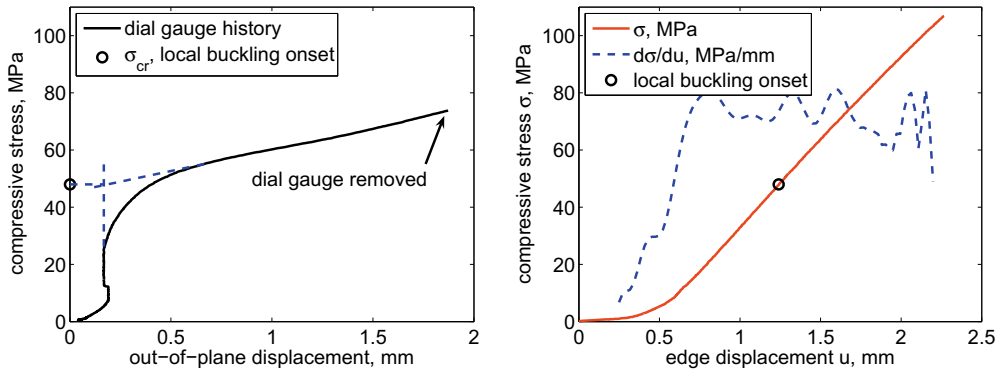

Fig. 8. Residual dent growth (left) and load–displacement response (right, the stiffness is fitted with a polynomial, since the original data show a large scatter) registered under edgewise compression. Configuration # 1, 60 J impact.

obvious because for the panels the progressive dent growth does not occur at the whole specimen width and is not accompanied by the overall bending, that occurs in this case in the beam specimens.

Face delamination resulted in its abrupt failure. This is observed for all configuration # 2 specimens. The failure occurs in a narrow through-the-width zone usually crossing the indented part of the face sheet and could thus be attributed to a stress concentration due to the residual dent. Small delamination at the former load site could also trigger the failure. Fig. 9 (left) shows a dependence dent magnitude (initial, after some growth at the moment of buckling, and ultimate) on the damage diameter. A prominent face dent growth is observed prior to the failure only in the specimens indented more than for 4 mm (having initial dent magnitude of 0.5 mm or higher).

For comparison, virgin specimens are tested also; configuration # 1 fails by wrinkling, and configuration # 2—by delamination. Thus, the failure mechanism of the tested panels remains unchanged if the damage covers a relatively small area (e.g. if the damage diameter is less than the wrinkle wavelength). Larger damage changes the failure mode for configuration # 1, while it remains the same for configuration # 2 (apparently, the dent growth only changes the bending stresses in the face sheet).

Fig. 9 (right) shows a reduction in the ultimate (at failure) stress, σ_{ult}, normalized to that of the virgin specimens, σ_{virgin}. As expected, strength in the wrinkling failure mode is not much dependent on the damage size. This is not the case when the final failure is provoked by the face delamination or dent growth. In this case, the dent magnitude as well as amount of the crushed core can significantly reduce the residual strength.

It is also seen that some normalized results are superior to 1.0. Probably this is just a statistical error caused by a small number of specimens. However when the same series (4–5) were used for sandwich beams [22], a similar effect was observed only once, and not for several points as in Fig. 9 (right). Another idea can be that the residual dent forms a small 3D geometrical 'stiffener'. If we then assume that the virgin and damaged specimens have the same ultimate edge displacement, then the latter may indeed have a higher ultimate strength. In the plane problem (beam specimens) the residual dent is 2D-shaped and thus does not stiffer the response.

The local buckling onset load is determined as the intercept between an extension of the region with stationary dent magnitude (almost no dent growth) and a tangent to the region of a progressive dent growth, measured by a dial gauge as shown in Fig. 8 (left). The results are presented in Fig. 10. For large damage sizes, the tests reveal a reduction factor in the buckling stress up to 2.3; the scatter is within 10%. If compare Fig. 10 (left) with Fig. 9 (right), it is seen that the ultimate failure load can noticeably be higher than the local buckling onset load. For example, the strength reduction factor after a 60 J impact is about 0.75; i.e., the strength is about 110 MPa, while the local buckling occurs at 65 MPa. For configuration # 2 this effect is milder, Fig. 10 (right), but it is anyway seen that the panels can undergo an increasing post-buckling load. It could be interesting to investigate is the post-buckling state is stable or not (due to creep and possibly other effects in the foam) under a constant overall load but this is beyond this paper.

As mentioned above, configuration # 1 panels most likely fail by the out-of-plane tensile fracture in the core somewhere at the boundary of the damage zone. This is prompted by the strain

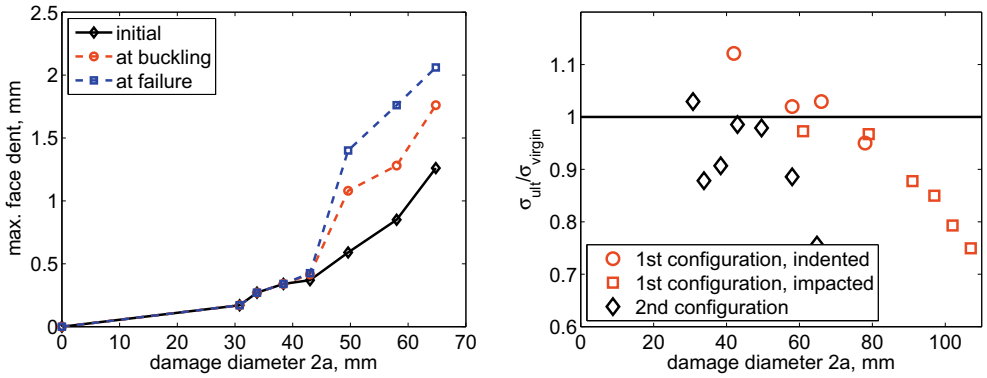

Fig. 9. Residual dent growth (left, configuration # 2) and ratio of the ultimate stress of damaged, σ_{ult}, and virgin, σ_{virgin}, panels (right) under edgewise compression, vs. the damage size.

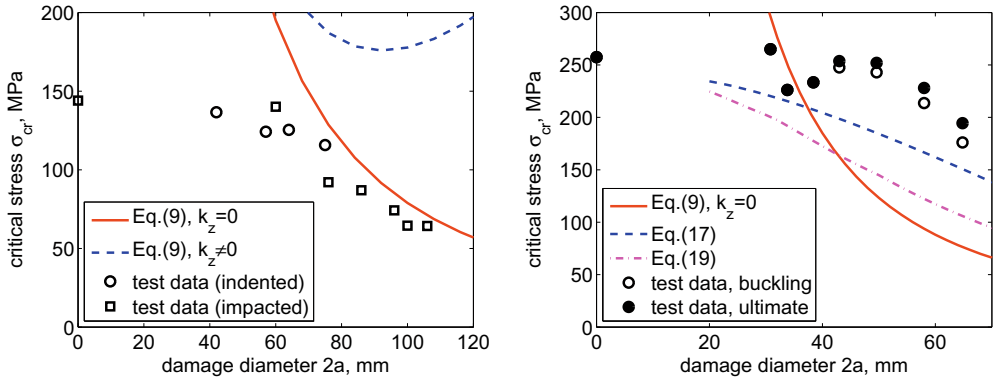

Fig. 10. Edgewise compression tests and theoretical results for configuration # 1 (left, test data for local buckling stress) or # 2 (right, the first four points give the ultimate stress only due to absent of buckling in these specimens).

gauges, which register a distinct strain decrease attributed to the local bending of the face sheet outwards the panel, while the inner area (the residual dent zone) bends inwards [20]. To clarify this phenomenon, the strain mapping is performed. Fig. 11 (left) shows the out-of-plane displacement field captured right before the final failure. The corresponding dent profiles are shown in Fig. 11 (right). Zones with positive (outward) displacements of the face sheet can be seen. "Bulges" in these zones increase simultaneously with the residual dent growth inwards. Prior the final failure, maximal outward displacement is about 0.64 mm.

Unfortunately, it is impossible to clarify if the failure initiates in the crushed or virgin core, since the local strains cannot be measured with any system used in this study. On one hand, a 0.64 mm deflection of the face sheet corresponds to a 1.3% nominal strain in the core. This value is very close to the ultimate tensile strain for virgin WF51 foam material. On the other hand, the "bulges" appear mostly within the core crush zone. In study [26], the pre-crushed WF51 foam specimens were tested in uniaxial tension until reaching their original (before crushing) length, and even in this case most of them fail prior to end of the test. In the present tests, it is obvious that the crushed core under the "bulges" undergoes much larger tensile deformation. However, all these considerations are very rough, since the real strains are apparently not uniaxial and not uniform through the core thickness. Also, the results from the tests on large foam specimens should not be scaled to the edge of the damage zone, where the crushed foam layer is thin and thus may not be considered as a continuum. Finally, the region of interest is a junction of virgin foam, crushed foam, and the cells filled with resin, which suggests the problem should be treated on the micromechanical level.

2.5. Crushed foam characterization

For modelling of the foam material, quasi-static uniaxial compression–tension is performed as shown in Fig. 12. First, the specimen is compressed until the foam is fully crushed, path *A–C* (path *A–B* represents the elastic response). This is followed by unloading and eventual loading in tension along path *C–D*. Then a constant strain $\varepsilon_D \equiv \varepsilon_E$ is kept for 10 min, while the stress follows path *D–E*. Finally, the specimen is compressed again, path *E–F*. The tests are performed for a number of different magnitudes of ε_E shown by circle markers in Fig. 12. Further details are reported in [26].

For the local buckling, mainly path *E–F* is important, since it characterizes the crushed core reaction during the inward growth of the face dent. This path contains two almost linear regions and can thus be approximated with two modules, E' and E'', as shown in Fig. 12 (right). Their values are dependent on the position of point *E*. In Table 2, the moduli are given for two extreme sets of the residual strain ε_E used in the tests. Taking a ratio between the maximal residual dent, w_0^r, and the damage depth, *d*, in the indented sandwich panels, Fig. 5, the average residual strain ε_E is estimated to be 0.08–0.17 or 0.08–0.13 for configurations # 1 and # 2, respectively. In the following, mean values of E' are used (contrary to the plane formulation, [22], path with E'' is not reached before the local buckling, due to minor growth of the residual dent).

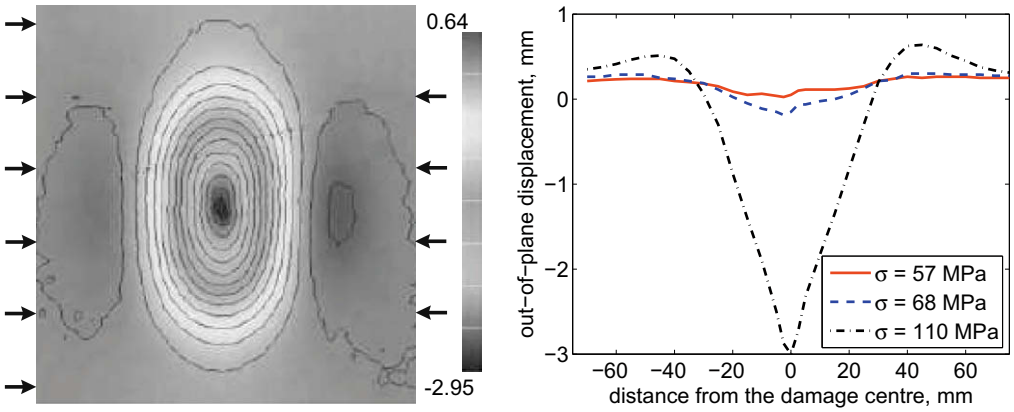

Fig. 11. Full-field displacement measurements under edgewise compression, around former 60 J impact site. Left: out-of-plane field (mm) prior to the failure ($\sigma = 110$ MPa, isolines are shown also). Right: face sheet profiles in the loading direction.

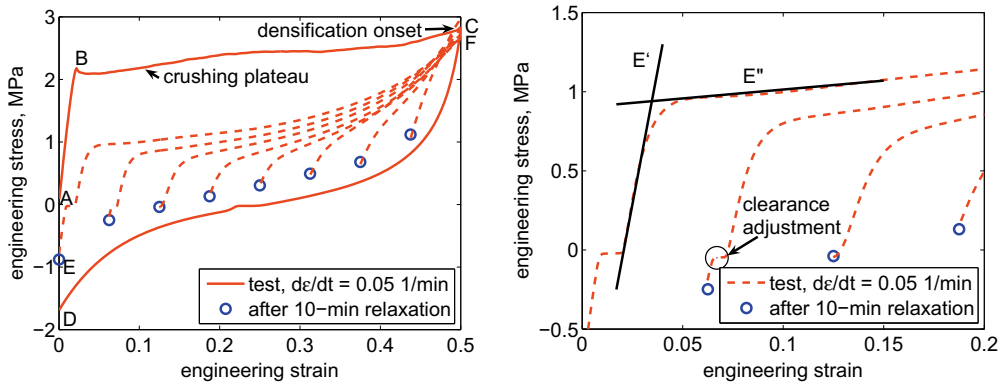

Fig. 12. Stress–strain curves in uniaxial compression/tension tests on H130 foam specimens; full-scale (left) and detail (right).

Table 2
Crushed core stiffness under secondary compression.

Configuration	Residual strain (ε_E)		Modulus E' (MPa)			Modulus E'' (MPa)		
	1	2	1	2	Mean	1	2	Mean
1	0.08	0.17	8.2	7.8	8.0	0.04	0.1	0.07
2	0.08	0.13	63.2	46.0	54.6	2.2	3.4	2.8

3. Theoretical

Reasoning from the experimental study, the theoretical approach is focused on (1) local buckling in the core crush zone and (2) compressive fracture of the face sheet. The wrinkling failure is not discussed, since its analysis requires an individual article [27]. It is worth to mention that the real wrinkling can occur much earlier than predicted by theory, mainly due to material non-linearity and a load eccentricity caused by tabs. This is the case for sandwich configuration # 1 tested in this study.

The face sheet over the core crush zone is modelled as a linear-elastic, non-stretchable, and elastically clamped plate having thickness h_f and bending stiffness D_f, Fig. 13. The clamp is used to model a reacting moment from the undamaged part of the sandwich. It is accepted also that $(h_f \ll (2a))$, so the thin plate Kirchoff–Love theory can be employed.

The stiffness D_f is constant; i.e., no damage of the face (delamination, fibre breakages) is considered. In the axisymmetric formulation (and similar 3D shape problems) it is almost the same for the stiffness response either one takes the virgin plate or reduces its stiffness in a small central area or even cuts this area off. Thus the face sheet damage should be accounted for only if covers a wide area; this is not the present case.

Two variants of the model are used below; $b = a$ and $b = 0$, Fig. 5. The first one, Fig. 13a, represents the case when there is a face–core debonding within the whole damage zone. The second one, Fig. 13b, includes a continuous support of the crushed core. The solutions given below are approximate, since "exact" closed-form solutions (if any) would be too complicated.

3.1. Local buckling

Consider bi-axial compression producing far-field stresses σ_x, σ_y; their critical (in the Euler sense, i.e., sufficient to keep a slightly bent form) values are to be determined. The particular case $(\sigma_x = \sigma_y)$ in Cartesian coordinates corresponds to uniform radial loading in the polar coordinates. The Ritz method can be utilized to solve this problem approximately. For this, a circular in-plane shape of the damage zone is substituted for a square one $(2a \times 2a)$; increased area results in a conservative estimation. Actually even the circular shape is a simplification, since initially circular residual dent zone becomes elliptical under uniaxial in-plane loading, Fig. 11 (left).

The residual face dent is disregarded, since the tests show that (1) the buckling profile is similar to the dent profile, (2) the dent is less than the face thickness, and (3) no considerable dent growth occurs prior to the buckling onset. As said above, the latter observation allows modelling of the crushed core as linear-elastic, with modulus E' introduced in Section 2.5. So the face keeps a straight form of equilibrium up to bifurcation, and the eigen mode is chosen as

$$w = (i\pi \sin(i\lambda x) + k \sin^2(i\lambda x))(j\pi \sin(j\lambda y) + k \sin^2(j\lambda y)) \qquad (2)$$

with $i, j = 1, 2 \ldots$, $\lambda = \pi/2a$, and $k = Ca/D_f$ that fits the elastic clamp condition

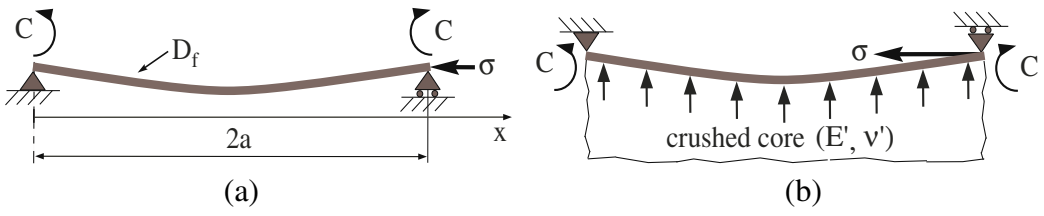

Fig. 13. Modelling approach for cases of (a) face–crushed core debond and (b) perfect interfacial bonding. Profile of the buckled face sheet is shown schematically.

at $x, y = 0, 2a$: $-D_f w'' = \mp C w'$. (3)

A conservative estimation of rotational stiffness C can be adopted from the plane problem, [22], (E_c is the Young's modulus of virgin foam material)

$$C \approx 0.2 h_f^2 \sqrt[3]{E_c E_f^2}. \quad (4)$$

The total energy is

$$\Pi = \frac{1}{2}\int_0^{2a}\int_0^{2a} (D_f(\triangle w)^2 + k_z w^2 - \sigma_x h_f (w'_x)^2 - \sigma_y h_f (w'_y)^2)\mathrm{d}x\mathrm{d}y + \frac{C}{2}\int_L (w'_n)^2 \mathrm{d}s, \quad (5)$$

where $\triangle = ()''_{xx} + ()''_{yy}$, L – plate contour, s – contour coordinate, n – normal line to the contour. The latter item can also be written as

$$\int_L (w'_n)^2 \mathrm{d}s = \int_0^{2a} \left((w'_x)^2|_{x=0} + (w'_x)^2|_{x=2a}\right)\mathrm{d}y + \int_0^{2a} \left((w'_y)^2|_{y=0} + (w'_y)^2|_{y=2a}\right)\mathrm{d}x. \quad (6)$$

The parameter k_z is the elastic foundation stiffness which represents a supporting effect of the crushed core. It can be estimated by matching (1) the "exact" Euler's stress for an infinite beam bonded to an elastic half-plane, [22,27], and (2) a similar solution where the half-plane is substituted for a Winkler foundation, [28],

$$k_z = \frac{9}{8\sqrt[3]{2}}\frac{D_f}{x_n^4}, \quad \bar{k_z} = \frac{k_z}{D_f}\left(\frac{a}{\pi}\right)^4. \quad (7)$$

The parameter x_n accounts here for the material properties,

$$x_n^3 = \frac{D_f}{E_1}, \quad D_f = \frac{E_f h_f^3}{12(1-\nu_f^2)}, \quad E_1 = \frac{2E'(1-\nu')}{(1+\nu')(3-4\nu')}, \quad (8)$$

where E' and ν' denote the Young's modulus and Poisson's ratio of the crushed foam material, assuming its isotropy. This is a conservative simplification of a real orthotropy [29]. The value of ν' can be accepted to be 0.3; its variation between 0.2 and 0.4 results in a negligible change of E_1.

Below for simplicity the particular case ($\sigma_x = \sigma,\ \sigma_y = 0$) is considered; this follows $j = 1$ for realizable eigen modes. Then substitution of approximation (2) into energy functional (5) with condition ($\Pi = 0$) produces

$$\sigma_{cr} = 2\phi\tilde{f} D_f / a^2 i^2 h_f \quad (9)$$

with $\phi = \pi^2/4$ and non-dimensional factor

$$\tilde{f} = \frac{(1+i^2)^2}{2} + \frac{3k(32+k(13+2i^2))/2}{48\phi + k(64+9k)} - \frac{6k^2(3\phi + k(10+3k))}{(48\phi + k(64+9k))(12i^2\phi + k(8\psi+3k))} + \frac{3ki^4(8+3k)/2 + 2\bar{k_z}(48i^2\phi + k(32\psi+9k))}{12i^2\phi + k(8\psi+3k)} \quad (10)$$

accounting for the crushed core support and elastic clamp stiffness. Here $\psi = 1-(-1)^i$. For the first eigen mode ($i = 1$) this simplifies into

$$\tilde{f} = \frac{\phi + 10k/3 + k^2}{\phi + 4k/3 + k^2/4} + \frac{\phi + 4k/3 + k^2/4}{\phi + 4k/3 + 3k^2/16} + 8\bar{k_z}\frac{\phi + 4k/3 + 3k^2/16}{\phi + 4k/3 + k^2/4}. \quad (11)$$

Results are shown in Fig. 10 for ($i = 1$) and cases with ($k_z = 0$) or without ($k_z \neq 0$) the cavity. These correspond to Fig. 13a or b, respectively. For configuration # 1 the agreement is very good between the estimation with ($k_z = 0$) and the test data. This is a natural result because (1) experimental points for the indented specimens lie on the left of the Euler's curve and (2) there is a large cavity in the impacted specimens. Thus the crushed core support is not important for the buckling behaviour in both cases, and the simplest solution with ($k_z = 0$) broadly works for them.

For configuration # 2 the theoretical solutions neither for ($k_z = 0$) nor for ($k_z \neq 0$) fit the test data. The obvious reason is a much stiffer crushed core support (54.6 vs. 8.0 MPa), Table 2. On the other hand, such a support rises the solution for ($k_z \neq 0,\ i = 1,2,3,4$) well above the test data even for the undamaged panels, Fig. 14 (left). Thus the failure is naturally dominated not by the local buckling but by a compressive failure in the face sheet, Section 2.4. A simplified solution for this case is presented below.

To verify Eq. 9, a simple linear-elastic FE analysis is performed for configuration # 2. Due to the symmetry of buckling across the load direction ($j = 1$), only half of the panel is modelled. This $200 \times 100 \times 40$ mm volume contains a $2a \times a \times 40$ mm prismatic core crush insert. Isotropic core layer and face sheet are meshed with tetrahedral or 3-node shell elements, respectively. The model is composed of eight elements through the core (condensed towards the face) and 40 elements lengthwise, i.e. a 5×5 mm mesh is created. A conservative compressive load is applied to the face sheet; only one translational degree of freedom is allowed for this edge of the model. All DOFs are fixed at the opposite edge as well as at the bottom edge of the core.

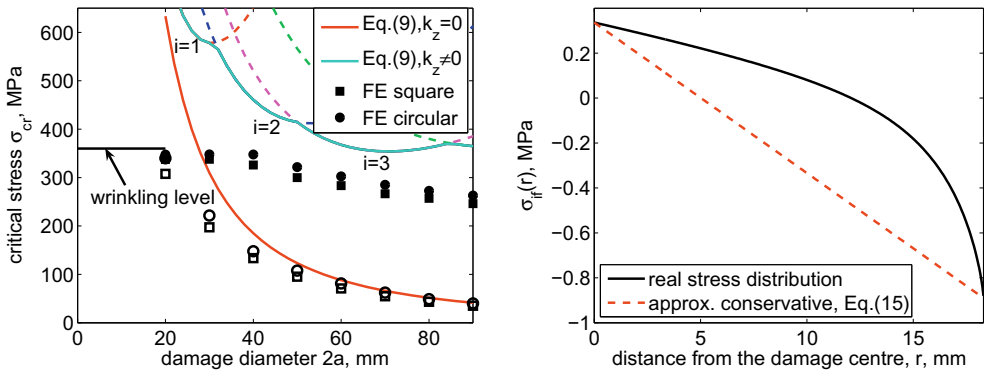

Fig. 14. Left: local buckling stresses for configuration #2 (solid markers for $k_z \neq 0$, empty ones for $k_z = 0$). The first two points for $k_z \neq 0$ correspond to the wrinkling behaviour. Right: distribution of the residual out-of-plane interfacial stress along crushed H130 core zone [25].

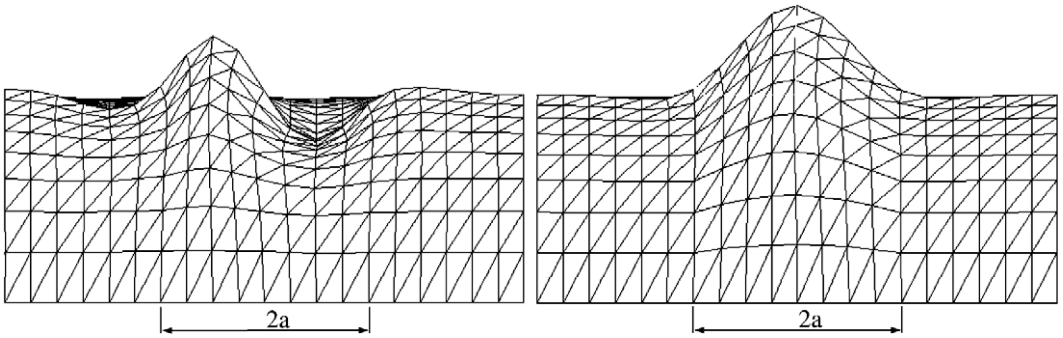

Fig. 15. Eigen modes in the FE model having a 40 × 40 mm square damage zone ($a = 20$ mm). Left: $k_z \neq 0$ ($E' = 54.6$ MPa). Right: $k_z = 0$ ($E' = 0.1$ MPa). Central part of the model is shown.

The obtained eigenvalues, Fig. 14 (left, square markers), are lower than the theoretical predictions. This discrepancy should mainly be due to the assumption of integer i within fixed face zone $2a \times 2a$ in Eq. 2, while the FE model allows for a more free buckling wave formation, Fig. 15 (left). This is prominent for this stiff ($E' = 54.6$ MPa) crushed core; if its support is eliminated ($k_z = 0$ or $E' = 0.1$ MPa in the FE model), the theory gives much better results, Fig. 14 (left), especially for large damage sizes, when the natural wavelength fits the damage size well, Fig. 15 (right).

A more realistic FE model having a cylindrical core crush zone of a radius a is tested also, Fig. 14 (left, circular markers). The results demonstrate a minor (less than 5%) discrepancy with the previous values, thus showing that a square damage zone is a good approximation of a circular one.

3.2. Compressive failure

Consider a circular region of the face sheet ($r < a$) perfectly bonded to the underlying crushed core, Fig. 13b. The case of a partial face–core debonding ($0 < b < a$) can be dealt with similarly, [25], but this is beyond the present study. For the area of interest, the stresses induced by the overall compression are accompanied by bending stresses. The residual dent profile is, as shown in [25],

$$wD_f = -\frac{pr^4}{64} - \frac{nr^5}{225} + A\frac{r^2}{4} + B \tag{12}$$

with

$$A = \frac{pa^2}{8}\frac{8k + k^*(k + 3 + \nu_f)}{(k + 1 + \nu_f)k^*} + \frac{2na^3}{45}\frac{15k + k^*(k + 4 + \nu_f)}{(k + 1 + \nu_f)k^*}, \tag{13}$$

where k^* is the cross stiffness parameter accounting for deflection due to rotation and vice versa, at the transition boundary ($r = a$) between the virgin and crushed core. For simplicity it is better to take $k^* = \infty$; this gives a negligible error for the present geometry and material configurations. This yields

$$A = \frac{pa^2}{8}\frac{k + 3 + \nu_f}{k + 1 + \nu_f} + \frac{2na^3}{45}\frac{k + 4 + \nu_f}{k + 1 + \nu_f}. \tag{14}$$

Parameters p and n result from a trapeziform model of a pull-in reaction of the crushed foam at the face–core interface, [25],

$$\sigma_{if}(r) = p + nr, \tag{15}$$

where p defines the reaction magnitude at the damage centre ($r = 0$) calculated using the crushed foam response in tension, Fig. 12; the corresponding strain is estimated using the test data for the crush zone depth, d, and maximal residual dent in the face, w_0^r, Fig. 5. The parameter n defines a linear variation of Eq. (15) towards the damage boundary ($r = a$). A conservative (resulting in larger pull-in reaction and therefore in higher bending stress) variant of n assumes that the residual strain in the crushed foam is zero at ($r = a$); this corresponds to point E in Fig. 12 (left). This choice results in the shape shown by a dashed line in Fig. 14 (right). The trapeziform model is adopted mainly because the real stress distribution depends on a particular sandwich constitution thus making a generalized form of the analytical solution impossible.

The radial bending moment

$$-D_f\left(w_{rr}'' + \nu_f\frac{w_r'}{r}\right) = \frac{pr^2}{16}(3 + \nu_f) + \frac{nr^3}{45}(4 + \nu_f) - \frac{A}{2}(1 + \nu_f), \tag{16}$$

produces maximal stress at ($r = 0$)

$$\sigma_r^{max} = -\frac{3}{2}\frac{D_f}{h_f^2}A(1 - \nu_f). \tag{17}$$

For the present case it can be assumed that the residual dent growth is negligibly small before the final failure, Fig. 9 (left). Therefore the local bending stress (17) is not much influenced by the overall compression. Then the total stress is calculated as their simple superposition, and the ultimate strength, σ_{ult}, is estimated by subtraction of (17) from the virgin panel strength, σ_{ult}^0. The results are shown in Fig. 10 (right) and agree with the test data.

A yet more conservative estimation accounts for the overall compression as

$$\sigma_{ult} = \sigma_{ult}^0 - \sigma_r^{max}\frac{\sigma_{cr}}{\sigma_{cr} - \sigma_{ult}} \tag{18}$$

(the factor is widely used for an approximate estimation of the deflections and stresses under a combined—in-plane and transversal—loading) or

$$\sigma_{ult} = (\sigma_{ult}^0 + \sigma_{cr})/2 - \sqrt{(\sigma_{ult}^0 + \sigma_{cr})^2/4 - \sigma_{cr}(\sigma_{ult}^0 - \sigma_r^{max})}, \tag{19}$$

where σ_{cr} is defined by Eq. (9). In the present case Eq. (19) gives an ultimate strength which is about 20% lower than follows from Eq. (17). As it is seen in Fig. 10 (right), due to many conservative assumptions solutions (17) and (19) give a significant underestimation of the residual strength but still can serve as a fast and rough approach to the problem.

4. Conclusions

The edgewise compression response of foam-cored sandwich panes with indent- or impact-induced damage is experimentally and theoretically investigated in this paper. The main results can be outlined as

- For the tested sandwich configurations, a typical damage consists of a sub-face core crush zone and residual dent in the face sheet. Almost no delamination is observed in the face. For the

sandwich configuration subjected to a low-velocity impact, the damage also contains a large interfacial cavity which considerably reduces the residual face dent;

- Under edgewise compression, the specimens having a small damage zone fail, depending on configuration, by abrupt wrinkling or compressive fracture of the face sheet. These failure modes coincide with the ones for virgin specimens of the same types and do not seriously alter the ultimate strength. When the damage size increases, the failure mechanism can change to a local buckling in the damage zone. This leads to a substantial reduction in the compression load capacity. If accompanied by a relatively large residual dent, the compressive fracture also occurs much earlier than in virgin panels;
- Three theoretical solutions predicting the ultimate residual strength are presented. The first solution assumes no support of the crushed core to the face sheet and thus gives a conservative estimation for the buckling load. The second, more refined solution, assumes a perfect bonding between the face and the crushed core and thus yields the upper limit of the buckling load. It is obtained that taking into account the supporting effect of the crushed core rises the critical load significantly. Here this effect is more prominent than for sandwich beams [22]. The third solution allows for prediction of the compressive failure of the face sheet due to overall compression and local bending stresses in the residual dent zone;
- The solutions demonstrate a good agreement with experimental and FE data, for a relatively large core crush zone. They may also be utilized for some sandwich configurations having corrugated or honeycomb cores.

Acknowledgements

Ms. Greet Kerckhofs (Katholieke Universiteit Leuven, Belgium) is gratefully acknowledged for the help with X-ray measurements. Authors would also like to thank Mr. Bo Magnusson, Mr. Peter Arfert, and Mr. Anders Beckman (Royal Institute of Technology, Sweden) for assistance with experiments. Some test specimens are kindly supplied by Dr. Per Wennhage (ibid).

References

[1] Rammerstorfer FG, Vonach WK. Wrinkling of thick orthotropic sandwich plates under general loading conditions. Arch Appl Mech 2004;70:338–48.
[2] Fagerberg L. Wrinkling of sandwich panels for marine applications. PhD thesis, Department of Aeronautics & Vehicle Engineering, Royal Institute of Technology, Stockholm, Sweden; 2003.
[3] Hayman B. Approaches to damage assessment and damage tolerance for FRP sandwich structures. J Sandwich Struct Mater 2007;9(6):571–96.
[4] Olsson R. Methodology for predicting the residual strength of impacted sandwich panels. Technical report FFA TN 1997-09. The Aeronautical Institute of Sweden (FFA), Stockholm; 1997.
[5] McGowan DM, Ambur DR. Damage characteristics and residual strength of composite sandwich panels impacted with and without compression loading. In: Proceedings of the 39th AIAA/ASME/ASCE/AHS/ASC structures, structural dynamics, and materials conference, Long Beach, USA, vol. 1; 1998. p. 713–23.
[6] Hansen U. Compression behavior of FRP sandwich specimens with interface debonds. J Compos Mater 1998;32(4):335–60.
[7] Cvitkovich MK, Jackson WC. Compressive failure mechanisms in composite sandwich structures. J Am Helicopter Soc 1999;44(4):260–8.
[8] Tomblin JS et al. Impact damage characterization and damage tolerance of composite sandwich airframe structures. Report FAA/AR-00/44, Wichita, USA; 2001.
[9] Moody RC, Harris JS, Vizzini AJ. Scaling and curvature effects on the damage tolerance of impacted composite sandwich panels. J Sandwich Struct Mater 2002;4(1):71–82.
[10] Lacy TE, Hwang Y. Numerical modelling of impact-damaged sandwich composites subjected to compression-after-impact loading. Compos Struct 2003;61(1–2):115–28.
[11] Olsson R. Energy criterion for dent growth in sandwich panels. In: Proceedings of the 6th international conference on sandwich structures (ICSS-6), Boca Raton, USA; 2003.
[12] Davies GAO et al. Compression after impact strength of composite sandwich panels. Compos Struct 2004;63:1–9.
[13] Bull PH, Edgren F. Compressive strength after impact of CFRP-foam core sandwich panels in marine applications. Compos. Part B 2004;35:535–41.
[14] Berggreen C. Damage tolerance of debonded sandwich structures. PhD thesis, Department of Mechanical Engineering, Technical University of Denmark, Lyngby, Denmark; 2004.
[15] Xie Z, Vizzini AJ. Damage propagation in a composite sandwich panel subjected to increasing uniaxial compression after low-velocity impact. J Sandwich Struct Mater 2005;7(4):269–88.
[16] Nøkkentved A, Lundsgaard-Larsen C, Berggreen C. Non-uniform compressive strength of debonded sandwich panels—I. Experimental investigation. J Sandwich Struct Mater 2005;7(6):461–82.
[17] Berggreen C, Simonsen BC. Non-uniform compressive strength of debonded sandwich panels—II. Fracture mechanics investigation. J Sandwich Struct Mater 2005;7(6):483–512.
[18] Avilés F, Carlsson LA. Experimenal study of debonded sandwich panels under compressive loading. J Sandwich Struct Mater 2006;8(1):7–31.
[19] Aminanda Y et al. Experimental and numerical study of compression after impact of sandwich structures with metallic skins. Compos Sci Tech 2009;69(1):50–9.
[20] Shipsha A, Zenkert D. Compression-after-impact strength of sandwich panels with core crushing damage. Appl Comp Mater 2005;12(3–4):149–64.
[21] Koissin V. The local strength of foam cored sandwich structures. PhD thesis, Department of Strength of Materials, State Marine Technical University, St.-Petersburg, Russia; 2004 [in Russian].
[22] Koissin V, Skvortsov V, Shipsha A. Stability of the face layer of sandwich beams with sub-interface damage in the foam core. J Compos Struct 2007;78(4):507–18.
[23] ROHACELL. Technical manual. Darmstadt: Röhm GmbH; 1987.
[24] DIVINYCELL. Technical manual H-Grade. Laholm: Divinycell Int. AB; 1995.
[25] Koissin V, Shipsha A. Residual dent in locally loaded foam core sandwich structures—analysis and use for NDI. Compos Sci Tech 2008;68(1):57–74.
[26] Koissin V, Shipsha A. Deformation of foam cores in uniaxial compression–tension cycle. J Sandwich Struct Mater 2006;8(5):395–406.
[27] Koissin V, Shipsha A, Skvortsov V. Effect of physical non-linearity on local buckling in sandwich beams. J Sandwich Struct Mater; in press.
[28] Hetényi MI. Beams on elastic foundation. Ann Arbor: University of Michigan Press; 1946.
[29] Koissin V, Shipsha A. Residual in-plane mechanical properties of transversely crushed structural foams. J. Sandwich Struct Mater 2009;11(2-3):199–211.